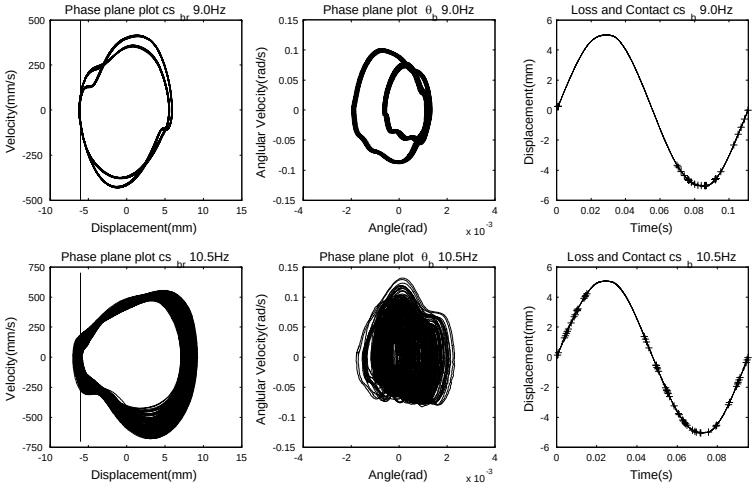

Figure 16. *Case 3*, 9.0Hz and 10.5Hz

Studying the signals from the laser measurements in figure 17, the beam centre's motion is seen to differ from the excitation's. The oscillation at 6Hz is recognised from other measurements as well, and is possibly caused by excitation of a natural frequency in the contact strip or the experimental rig. To be able to conclude the actual reason for this behaviour, an additional measurement of the excitation beam's ends would need to be performed.

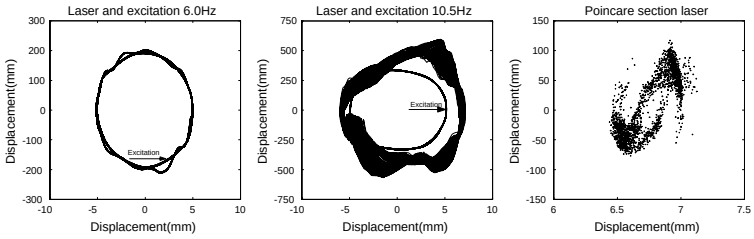

Figure 17. *Case 3*, 6.0Hz and 10.5Hz

The jumps in the velocity field, at 10.5Hz, has its origin in the impacts with the excitation, and since it is uncertain whether the excitation signal corresponds to the actual movement at the excitation point of the beam, no adjustment of the laser displacement's zero level has been performed. The Poincaré section reveals the fractal structure of the attractor and argues for a chaotic motion of the strip.

6 Modelling and Simulation

6.1 Mathematical Model

The mathematical model represents the head assembly, when fixed to ground, without considering the importance of the frame assembly, and corresponds to the experimental *Case 3*. The reason to restrict the model to the head assembly, with only one contact strip, is that it is desirable to find out whether a simple model could be used to get a better understanding for the underlying reasons of the pantographs complex behaviour.

The model is built up by a rigid beam, with vertical and rotational freedom around its centre of mass, suspended at its ends in suspension elements, as seen in figure 18. The suspensions are built up by piecewise linear springs, friction and viscous damping elements.

The piecewise linearity of the springs is introduced into the model by the additional springs placed at each side of the beam's ends. The upper limit is reached when the beam is displaced by x_u in upward direction about its equilibrium position, with the corresponding stiffness k_u, and the lower limit at x_l in downward displacement, with stiffness k_l.

The friction force is modelled by a tangents hyperbolic function, to soften up the step change in friction force, so that the numerics run more efficient and the viscous damping with a cosine hyperbolic function in the denominator. The cosine hyperbolic function causes a decrease in damping force with increased velocity, and is a result of fitting the numerical results to the experimental.

The beams angular displacement is assumed to be small, whereby linearization of the equations has been performed, and the forces acting in the horizontal direction are neglected.

To include the beam centre's oscillation, present in the phase plane orbits from the experimental measurements as seen in figure 17, an additional mass, m_2 , with vertical freedom, is added at the beam centre. Its mass and spring stiffness is matched with a natural frequency in the beam, found at 50Hz.

The excitation of the model is sinusoidal and applied at the beam centre through a stiff mass-less spring and damper element, which applies a force to the mass, m_2, when in contact with the excitation, and allows loss of contact and impact.

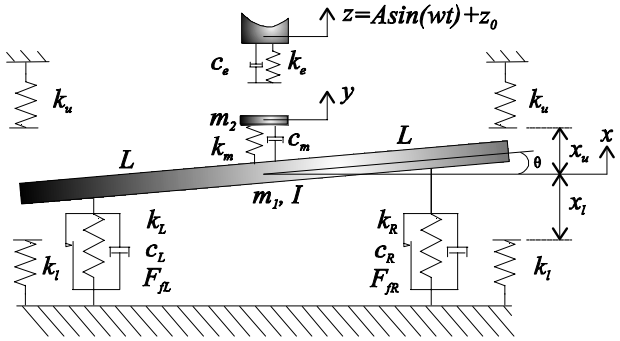

Figure 18. Schematic drawing of the mathematical model, with significant parameters

The mathematical model can be derived using four ordinary differential equations and switching conditions, when loss or impact occurs at the excitation as well as at the upper- and lower limits:

$$\ddot{\theta} = L(F_L - F_R)/I \tag{1}$$
$$\ddot{x} = (F_m - F_L - F_R)/m_1 \tag{2}$$
$$\ddot{y} = (-F_m - F_{impact})/m_2 \tag{3}$$
$$z = A\sin(wt) + z_0 \tag{4}$$

where

$$F_L = x_L \cdot k_L + \dot{x}_L \cdot c_L/\cosh(\dot{x}_L \cdot \alpha) + F_{f_L} \cdot \tanh(\dot{x}_L \cdot \beta) + F_{k_{Ll}} + F_{k_{Lu}} \tag{5}$$
$$F_R = x_R \cdot k_R + \dot{x}_R \cdot c_R/\cosh(\dot{x}_R \cdot \alpha) + F_{f_R} \cdot \tanh(\dot{x}_R \cdot \beta) + F_{k_{Rl}} + F_{k_{Ru}} \tag{6}$$
$$F_m = k_m \cdot x_{yx} + c_m \cdot \dot{x}_{yx} \tag{7}$$
$$F_{impact} = \begin{cases} -k_e \cdot x_{zy} - c_e \cdot \dot{x}_{zy} \text{ when } x_{zy},\ \dot{x}_{zy}<0, \\ -k_e \cdot x_{zy} \text{ when } x_{zy} < 0 \text{ and } \dot{x}_{zy}>0, \\ 0 \text{ when } x_{zy}>0 \end{cases} \tag{8}$$

and

$$F_{k_{Ll}} = (x_L + x_l)k_l \text{ when } x_L < x_l \text{ otherwise } F_{k_{Ll}} = 0 \tag{9}$$
$$F_{k_{Rl}} = (x_R + x_l)k_l \text{ when } x_R < x_l \text{ otherwise } F_{k_{Rl}} = 0 \tag{10}$$
$$F_{k_{Lu}} = (x_L - x_u)k_u \text{ when } x_L > x_u \text{ otherwise } F_{k_{Lu}} = 0 \tag{11}$$
$$F_{k_{Ru}} = (x_R - x_u)k_u \text{ when } x_R > x_u \text{ otherwise } F_{k_u} = 0 \tag{12}$$
$$x_L = x - \theta \cdot L \tag{13}$$
$$x_R = x + \theta \cdot L \tag{14}$$
$$x_{yx} = y - x \tag{15}$$
$$x_{zy} = z - y \tag{16}$$

6.2 Nomenclature

m_1	Beam mass (kg)
I	Beam mass moment of inertia (kgm^2)
L	Distance between beam centre and suspension
k_L/k_R	Spring stiffness coefficient left/right suspension (N/m)
c_L/c_R	Viscous damping coefficient left/right suspension (Ns/m)
F_{f_L}/F_{f_R}	Friction force coefficient left/right suspension (N)
k_u/k_l	Spring stiffness coefficient upper/lower limit (N/m)
x_u/x_l	Distance between upper/lower limit and the beam's equilibrium position (m)
m_2	Beam mass2 (kg)
k_m	Spring stiffness coefficient mass2 suspension (N/m)
c_m	Viscous damping coefficient mass2 suspension (Ns/m)
k_e	Spring stiffness coefficient excitation suspension (N/m)
c_e	Viscous damping coefficient excitation suspension (Ns/m)
z_0	Displacement of the excitation's zero level about the strips equilibrium (m)

6.3 System Specification

The parameters used in the numerical simulations comes from section 3 and the excitation suspension an approximation to yield a stiff impact, with values presented in table 2.

Parameter	Value	Parameter	Value
m_1	$3kg$	F_{f_R}	$1.6N$
I	$0.78kgm^2$	k_u	$47500N/m$
L	$0.58m$	k_l	$7550N/m$
k_L	$1150N/m$	x_u	$0.002m$
k_R	$1150N/m$	x_l	$0.029m$
c_L	$10Ns/m$	m_2	$0.5kg$
c_R	$16Ns/m$	k_m	$50000N/m$
α	40	c_m	$50Ns/m$
β	10000	k_e	$150000N/m$
F_{f_L}	$1N$	c_e	$150Ns/m$
A	$0.005m$		

Table 2. The Parameters for the numerical model

6.4 Numerical Results

Two different cases, comparable with the experimental, are considered in the numerical analyses of the model built. The first *Case A* is to be compared with the experimental results from *Case 1* and 3, where impact with the lower limit could occur, with a z_0=0.022m causing a pre-load in each suspensions of F_p=25.3N. In the second *Case B*, one side of the beam is allowed to impact at the upper limit, as in the experimental *Case 2,* and a z_0=0.005m used, resulting

in a preload of F_p=5.75N. The initial conditions for the two cases are seen in table 3, and the equations solved using the Matlab software package's ode45 solver with a relative and absolute tolerance of $1 \cdot 10^{-9}$.

Case	$x(0)$	$\dot{x}(0)$	$\theta(0)$	$\dot{\theta}(0)$	$y(0)$	$\dot{y}(0)$
A	-0.022	$A \cdot w$	0	0	-0.022	$A \cdot w$
B	-0.005	$A \cdot w$	0	0	-0.005	$A \cdot w$

Table 3. The initial conditions for the numerical model

6.4.1 Case A

The first results, presented in figure 19, clearly visualize the frictional effects in the suspensions and the up- and downward symmetry previously seen in the measurements. The contact at the excitation remains and no impact at the lower limits occur. If compared with the results in figure 13 they show very much the same behaviour.

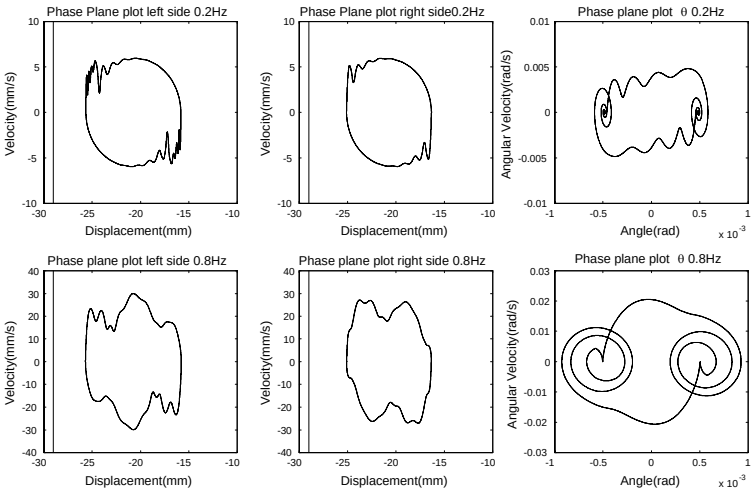

Figure 19. *Case A*, 0.2Hz and 0.8Hz

The same yields the results in figure 20, to be compared with the experimental results found in figure 14 where the behaviour occurs at a slightly higher frequency.